INTERACTION BETWEEN AN AIR ASSISTED JET
AND AN ACOUSTIC FIELD

G. Boisdron, F. Baillot, C. Dumouchel, J.-B. Blaisot

CORIA, UMR 6614 Université de Rouen
Site universitaire du Madrillet
BP 12 Avenue de l'université
76801 St-Etienne du Rouvray Cedex
e-mail : Gilles.Boisdron@coria.fr

ABSTRACT

High frequency combustion instabilities due to the presence of transverse acoustic perturbations have to be understood to ensure a safe working and high performances of rocket engines. In this framework, the present experimental study investigates the possible coupling between the spray formation and an acoustic field that could feed these instabilities. To achieve this, the behaviour of an air-assist liquid jet placed in a standing transverse acoustic field is studied. The experimental set-up allows reaching injection conditions usually encountered in rocket engines (We_g<3 300, Re_l<6 000) and the pressure fluctuations can reach 3 600 Pa, *i.e.*, 3 % of the mean ambient pressure. Visualisations of the injection are performed using different techniques. It is found that the disintegration process of the liquid jet can be very much affected by the acoustic field provided that the Weber number is smaller than 60. The influence of the acoustic field on the atomisation process is a function of the injection conditions (liquid and gas velocity), the position of the jet in the field as well as the acoustic field intensity.

1. INTRODUCTION

In rocket engines, instabilities that could lead to the destruction of combustion chambers are frequently encountered [1]. These instabilities result from the coupling between the pressure waves and the heat release rate. They can be classified in three families (system, chamber and combustion intrinsic instabilities) [2]. The one of interest in this paper is linked to the transverse resonant modes of the combustion chamber, characterised by a frequency of a few kilohertz. So far, the coupling between pressure waves and heat release rate is badly understood for now, due to the number and the complexity of the phenomena involved (injection, atomisation, reactant mixing, *etc.*). This paper focuses on the effect of a high-amplitude standing acoustic wave at 1 000 Hz on the atomisation process of an air-assist jet whose injection conditions are typically those encountered in rocket engines (We_g<3 300, Re_l<6 000).

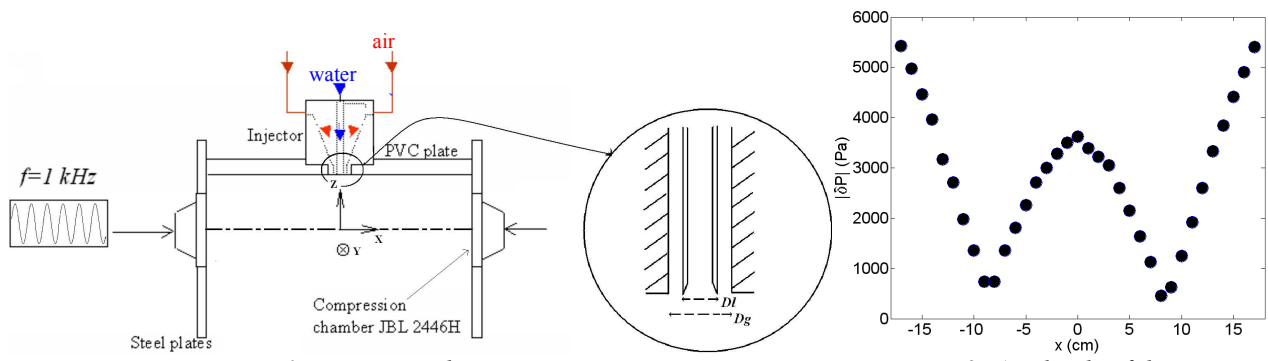## 2. EXPERIMENTAL FRAMEWORK & GENERAL BEHAVIOUR

Figure 1: experimental apparatus

Figure 2: Amplitude of the pressure field inside the cavity (on the loudspeaker axis)

Figure 1 presents the experimental setup. A standing wave is created between two loudspeakers mounted on steel plates parallel to the vertical injection axis and facing each other. Thus, the wave plane is parallel to the *Y-Z* plane *i.e.* transverse to the two-phase flow. The distance between the plates is fixed to 360 mm to obtain a resonance giving a maximum pressure fluctuations amplitude at *X*=0 for the excitation frequency *f*=1 000 Hz. The amplitude of the pressure field inside the cavity is shown in Fig. 2. The acoustic field presents an anti-node at *X*=0 between two nodes at
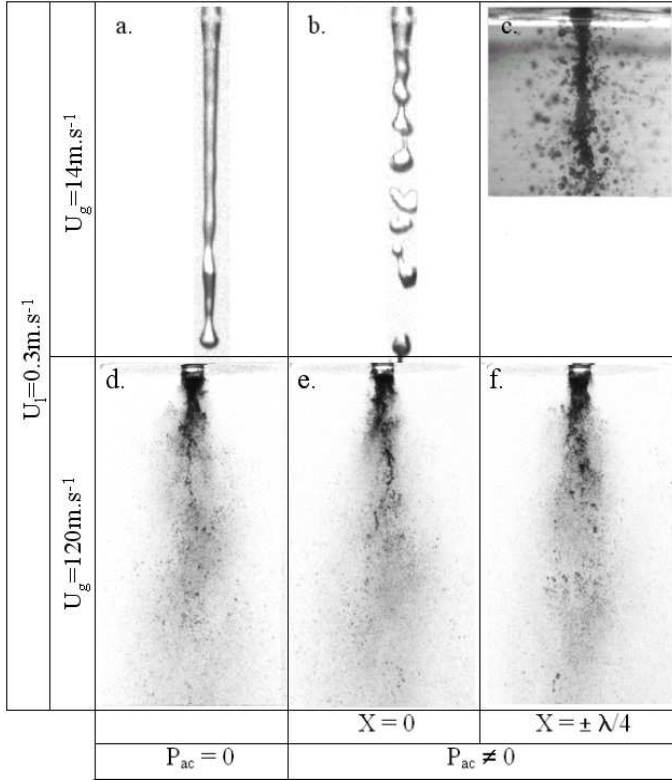
Figure 3: Backlight visualisations for different flow conditions (reported in the margin). The left column is for reference (without acoustics). Middle and right columns show the effect of acoustics on the atomisation process.

$X=\pm\lambda/4$ along the X direction. The acoustic level in the cavity is referred by P_{ac}, the absolute value of the acoustic pressure amplitude at the centre of the cavity ($X=Y=Z=0$).

Levels greater than 180 dB are reached in rocket engines. These levels correspond to pressure fluctuations amplitude about 10 % of the pressure inside the combustion chamber. Coupling between acoustic fluctuations and jets have already been mentioned in laboratory experiments for acoustic pressure levels around 140 dB [3]. The maximum acoustic pressure fluctuations reached in our experiments is P_{ac}=3 600 Pa, which corresponds to a sound pressure level of 163 dB and an amplitude of acoustic pressure fluctuations equal to 3 % of the mean ambient pressure.

A coaxial injector is used to create the two-phase flow. Water is injected at the centre from an orifice of diameter D_l=5.8 mm and the surrounding airflow is characterised by internal and external diameters D_{gi}=6 mm and D_g=8 mm respectively. The internal nozzle for the water flow is divergent at its exit as detailed in Fig. 1. The range of mass-average velocities is $0<U_l<1$ m.s^{-1} for the water and $0<U_g<175$ m.s^{-1} for the air. The injector is placed either at a pressure anti-node (X_{inj}=0) or at a pressure node (X_{inj}=$\pm\lambda/4$). For X_{inj}=0 the flow is exposed to acoustic pressure fluctuations, and for X_{inj}=$\pm\lambda/4$ it is exposed to acoustic velocity fluctuations [4].

Figure 3 presents backlight visualisations of jets with and without acoustics for different flow conditions. The left column of the Fig. 3 presents examples of jets without acoustics. The range of gaseous Weber numbers and liquid Reynolds numbers covered in our test rig are: $0<We_g<3$ 300 & $0<Re_l<6$ 000. Break-up processes observed here are from Rayleigh jet break-up (Fig. 3.a) to fiber type atomisation (Fig. 3.d), as introduced by Lasheras and Hopfinger [5].

The lower row of Fig. 3 presents cases corresponding to fiber type atomisation (*i.e.* $We_g>1$ 000). The images of Figs. 3.d, 3.e and 3.f are rather similar, *i.e.* the effect of acoustics is not obvious on these pictures. Conversely, for low Weber numbers ($We_g<60$), the acoustics clearly acts on the large scales of the jet as can be seen on the upper row of Fig. 3. The present study focuses on these situations only. Future works will be carried out for the case of high airflow rates ($We_g>60$) through the characterisation of the wavelengths on the liquid interface or of the droplet diameter distributions.

Comparison between Figs. 3.a and 3.b shows a slight modification of the break-up process when acoustic pressure fluctuations are generated (X_{inj}=0 –*i.e.* pressure anti-node). This has been quantified through the measurement of the break-up length (L_{bu}), defined by the length of continuous portion of the jet measured from the nozzle exit up to the break-up point [6]. Measurements of the break-up length are realised by image processing [7]. High-resolution images are recorded with a Kappa DX2N CCD camera (1 384×1 032 pixels, 12bits). For each flow condition, the mean break-up length is measured from 300 images. The effect of the flow conditions (U_l, U_g) and of the pressure fluctuations (P_{ac}) on the break-up length is reported in the next two sections.

Comparison between Figs. 3.a and 3.c shows that acoustic velocity fluctuations deeply modify the atomisation process, with production of drops near the nozzle outlet. The progressive development of this new atomisation process is presented in section 5. Time-resolved visualisations of this process are achieved with a Kodak Ektapro HS-4540 camera (256×256 pixels, 8bits, 4 500 f/s).

3. JET WITHOUT ACOUSTICS

Figure 4 presents the variation of the jet break-up length L_{bu} as a function of the liquid velocity for different values of the surrounding airflow velocity. Referred in the literature as the stability curve, the variation of the break-up length with the liquid velocity is often used to characterise the behaviour of cylindrical liquid jets (see [7] for instance). However, as far as we know, jet stability curves have never been reported for air assisted cylindrical liquid jets.

For U_g=0, Fig. 4 shows that the break-up length increases as the jet velocity increases, reaches a maximum and decreases towards an asymptotic value of the order of 45 D_l. The break-up length is maximum when the jet velocity is equal to 0.3 m/s and the asymptotic behaviour is reached for a liquid velocity of the order of 0.4 m/s. For the liquid velocity range examined here, *i.e.* [0.1 m/s; 0.8 m/s], the liquid jet is subject to the Rayleigh instability with the growth of a varicose perturbation up to the disintegration of the jet into drops of diameter roughly twice the jet diameter. The

stability curve obtained here in the absence of gas stream around the liquid jet is slightly different than the one usually reported for a capillary jet, *i.e.* a jet with a small diameter (less than 1 mm, see [7] for instance). For capillary jets, the maximum in L_{bu} is followed by a continuous decrease, a minimum and a second zone of increase when the jet velocity increases. A zone of constant L_{bu} as the one reported in Fig. 4 has never been reported. This specific behaviour is likely to be related to gravity whose effects can no longer be neglected for large jets as the one investigated here. Furthermore, the maximum L_{bu}, characterised by a so small Weber number (We_g=0.01), is not the consequence of aerodynamic effects as it could be for capillary jets [7].

The presence of an airflow around the cylindrical liquid jet modifies the stability curve. For U_g=3.5 m/s, Figure 4 shows slightly reduced break-up lengths provided that the liquid velocity is less than 0.4 m/s. For this range of liquid velocities, L_{bu} is less than in the absence of airflow and it increases continuously with the liquid velocity without exhibiting a maximum. However, for liquid velocities greater than 0.4 m/s, the influence of the airflow is negligible: L_{bu} is constant and of the order of 45 D_l as in the previous case. Finally, it can be added that for U_g=3.5 m/s, the disintegration process observed on the jets remains unchanged compared to the case with no airflow.

For greater gas velocities (U_g=14 m/s and 17.5 m/s), Figure 4 shows that the presence of the airflow affects much more the jet stability curve. From a general point of view, an increase of the airflow velocity induces a decrease of the break-up length whatever the liquid velocity. For U_g=14 m/s, a quasi-linear relationship is obtained between the break-up length and the liquid velocity. For U_g=17.5 m/s, the break-up length is almost constant when the liquid velocity varies from 0 to 0.4 m/s and then shows a linear increase. Note that the linear dependencies observed at U_g=14 m/s and U_g=17.5 m/s report equivalent slopes. Furthermore, it must be pointed out that the reduction of the break-up length comes with a change of the jet disintegration process from Rayleigh break-up to asymmetric Rayleigh break-up. This was observed here for the situations that reported a break-up length less than 10 D_l. For these cases that correspond to a high airflow velocity and to a small liquid velocity, the liquid column is subject to the growth of a sinuous perturbation and disintegrates into drops with a diameter much smaller than in the symmetric Rayleigh process. Thus, as expected, the airflow promotes the liquid jet atomisation by reducing the break-up length and the drop diameter, when the gasflow velocity is sufficiently high compared to the liquid velocity.

4. JET AT THE PRESSURE ANTI-NODE (X_{inj}=0)

Figure 5 presents the influence of an acoustic field on the stability curves presented in the previous section when the jet is positioned at the pressure anti-node X_{inj}=0 (see Fig. 2). These results were obtained for a constant acoustic level P_{ac}=3 200 Pa.

It must be first observed that the jet stability curve appears independent of the presence of an acoustic field when no airflow assists the liquid jet atomisation. However, when the airflow velocity is no longer zero, the acoustic field influences the jet break-up length. This influence is a function of both the liquid and air velocities.

When U_g=3.5 m/s, two stability curves were obtained according to the way the acoustic amplitude of 3 200 Pa is approached. When P_{ac} is increased from 0 to 3 200 Pa, the upper curve in Fig. 5 is obtained. For this case, the liquid jet reports the same atomisation process as the one observed in the absence of acoustic field, *i.e.* the jet break-up results from the growth of a varicose perturbation (Rayleigh instability). In this situation, the acoustic field reduces the break-up length when the liquid velocity is less than 0.6 m/s. For greater liquid velocities, the break-up length is identical to the one obtained in the absence of acoustic field. When P_{ac} is decreased from 3 500 Pa to 3 200 Pa, the lower curve in Fig. 5 is obtained indicating a stronger influence of the acoustic field on the break-up length. For this case, the atomisation process of the liquid jet is different than the one reported in the absence of acoustics. Indeed, a sinuous perturbation deforms the jet and small droplets are ejected right at the nozzle exit. This droplet ejection phenomenon is
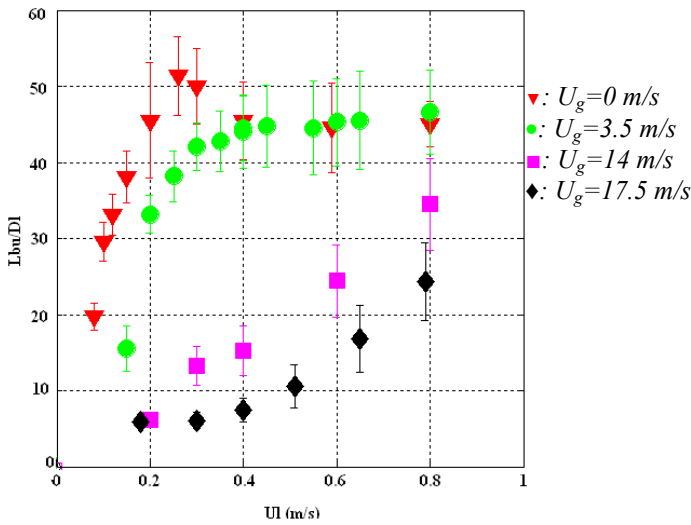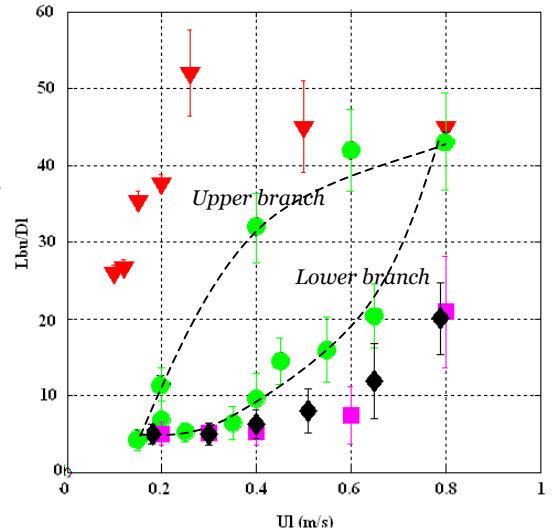
Figure 4: Stability curve of air-assist jets.

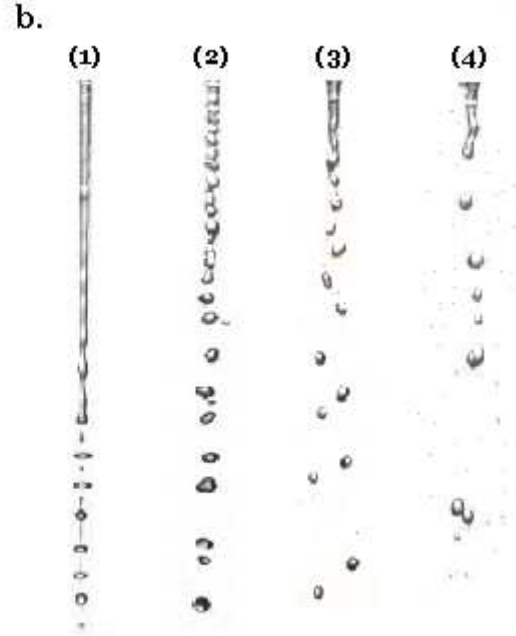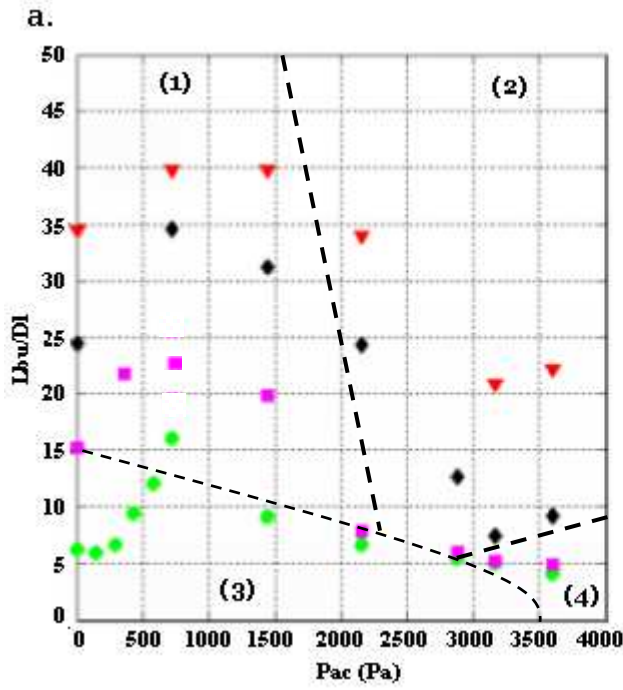Figure 5: Influence of acoustic perturbations on the jet stability curve for P_{ac}=3 200 Pa and X_{inj}=0.

Figure 6: Effect of the acoustic amplitude at the pressure anti-node ($X_{inj}=0$) for $U_g=14$ m.s^{-1}, •: $U_l=0.2$ m.s^{-1}; ■: $U_l=0.4$ m.s^{-1}; ♦: $U_l=0.6$ m.s^{-1}; ▼ : $U_l=0.8$ m.s^{-1} on (6.a): the break-up length (the dashed lines limit morphological zones described in 6.b); (6.b) the morphology of jets.

pulsed. A closer look at the nozzle shows that the jet completely wets the nozzle lip. Furthermore, a temporally growing but spatially damped disturbance is observed. When the amplitude of this disturbance in high enough, the co-flowing air stream peels off droplets.

For higher airflow velocities, only one stability curve is obtained whatever the way the acoustic amplitude of 3 200 Pa is reached. For $U_g=14$ m/s, the break-up length is not influenced by the acoustic field when $U_l=0.2$ m/s and L_{bu} is reduced for $U_l>0.2$ m/s. For $U_g=17.5$ m/s, L_{bu} is reduced for $U_l>0.4$ m/s. Note that above this liquid velocity, the break-up length increases linearly with the liquid jet velocity as in the case without acoustics. However, this relationship is characterised by a lower slope. In conclusion, Fig. 5 shows that an acoustic field reports an influence on the liquid jet break-up length provided that the break-up length of the natural jet (without acoustics) is a function of both the air and liquid velocities. This is why no influence of the acoustic field is reported when $U_g=0$.

The influence of the acoustic field on the jet break-up length is also a function of the acoustic amplitude P_{ac}. This is illustrated in Fig. 6a that reports the variation of the break-up length versus P_{ac} for a constant airflow velocity ($U_g=14$ m/s) and different liquid jet velocities (from 0.2 m/s to 0.8 m/s). This figure shows that, whatever the liquid velocity,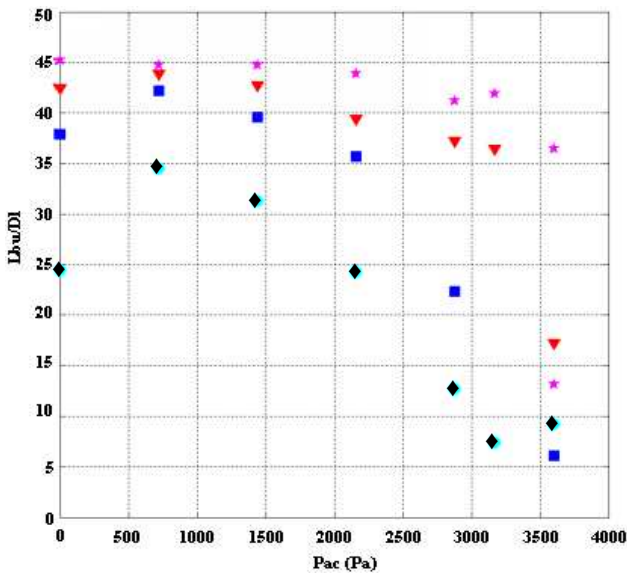 a small P_{ac} may stabilise the liquid jet. Indeed, when P_{ac} increases from 0, the break-up length increases, reaches a maximum and decreases. For the different situations examined here, the maximum in break-up length is reached for P_{ac} ranging from 500 to 1500 Pa according to the liquid velocity. Furthermore, Fig. 5 indicates that the acoustic field influences the break-up length as well as the atomisation process. Four different atomisation regimes were identified. An example of each of them is shown in Fig. 6b. As said above, in the absence of acoustic field, two atomisation regimes are identified: the Rayleigh and the sinuous modes ((1) and (3) in Fig. 6b respectively). For a constant airflow velocity of 14 m/s, the sinuous mode is obtained for the smallest liquid velocity (0.2 m/s) and the Rayleigh mode is observed for the three greatest liquid velocity (see Fig. 6a). When the break-up length decreases under the action of the acoustic field, these atomisation regimes are replaced by two other regimes. Globally speaking, the Rayleigh mode changes in the atomisation regime (2) shown in Fig. 6b. For this regime, the jet perturbation is still rather axisymetric and the drops are produced on the

Figure 7: Effect of the acoustic amplitude at the pressure anti-node ($X_{inj}=0$) for $U_l=0.6$ m.s^{-1}. ★: $U_g=3.5$ m.s^{-1}, ▼ : $U_g=7$ m.s^{-1}, ■: $U_g=10.5$ m.s^{-1}, ♦: $U_g=14$ m.s^{-1}

jet axis. The size of the drops is of the same order as those produced by the Rayleigh mode. They are greater than the jet diameter. The main difference between regime (1) and (2) is the early perturbation of the liquid jet. Indeed, as soon as the liquid issues from the nozzle, a varicose disturbance is observed on the liquid jet interface. Similarly, the atomisation regime (3) changes in the atomisation regime (4) when P_{ac} increases (see Fig. 6a). This fourth atomisation regime is the one described above with sinuously perturbed jet and a pulsed drop ejection at the nozzle exit.

The influence of the acoustic field on the jet break-up length and atomisation regime is a function of the airflow velocity also as shown in Fig. 7. This figure presents the variation of the break-up length versus P_{ac} for a constant liquid velocity (U_l=0.6 m/s) and different airflow velocities (from 3.5 m/s to 14 m/s). It can be shown that the stabilising effect of the acoustic field depends on the airflow velocity. Indeed, no maximum break-up length is obtained when P_{ac} increases from 0 when the airflow velocity is small. However, for higher airflow velocities, the stabilising effect of the acoustic field arises at a constant P_{ac} of the order of 700 Pa. Thus, it can be concluded here that the acoustic level at which the break-up length is maximised is mainly a function of the liquid jet velocity.

This part of the work shows that the behaviour of an air assisted liquid jet is affected by an acoustic field when the jet is positioned at a pressure anti-node. This influence concerns the jet break-up length as well as the atomisation process and is a function of both the airflow and the liquid velocities and of the acoustic level.

5. JET AT A PRESSURE NODE (X_{inj}=±λ/4)

This part describes and analyses first results concerning the behaviour at a pressure node (X_{inj}=±λ/4). Preliminary experiments at P_{ac}=3200 Pa, discussed here, were performed for two kinds of conditions: U_g=0 m/s and 0.2<U_l<0.8 m/s; 0<U_g<175 m/s and U_l=0.3 m/s. Examples of the jet behaviour are presented in Fig. 7 for U_g=0 m/s and U_l=0.2, 0.6 and 0.8 m/s. These visualisations were realised 40° off-axis. They show an oval liquid sheet with a high atomisation level (behaviour observed for all the liquid velocities and U_g<25 m/s). The distance L_s from the nozzle exit to where the sheet begins to develop increases as the liquid velocity increases. For U_l<0.3 m/s, L_s=0 and for U_l>0.3 m/s L_s varies linearly with U_l: L_s=5.10^{-3} U_l. Two atomisation processes are observed: atomisation of sheet rims creating large drops and atomisation of the sheet itself ejecting small droplets perpendicularly to the sheet.

In order to understand the appearance of the sheet and its atomisation, a time-resolved study in the XZ plane is presented in Fig. 8 for U_g=14 m/s and U_l=0.3 m/s. Note that the acoustic field in the cavity needs 30 ms to become stationary after the beginning of sound emission (τ=0) at 1 kHz, where τ is the time after the start of acoustics. For 0<τ<30 ms, the amplitudes of pressure and velocity fluctuations rise quasi-linearly. When τ=0 (Fig. 8.a), the jet is not acoustically perturbed. At τ=17 ms (Fig. 8.b), the jet shows a contraction in the X direction. Its width in this direction is divided by two. Off-axis visualisations, not shown here, indicate that this co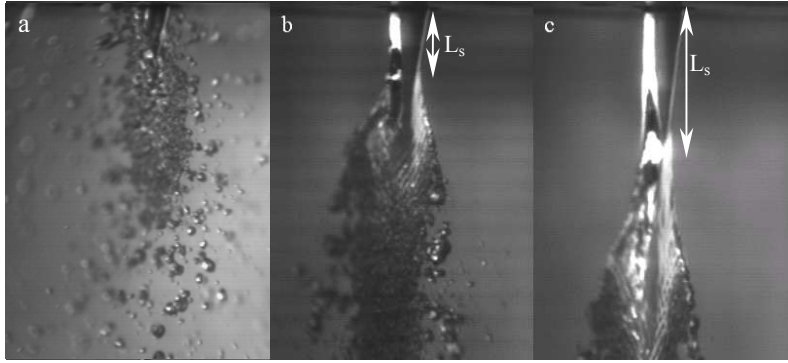ntraction comes with a dilatation in the perpendicular plane YZ. At τ=31 ms (Fig. 8.c), an asymmetric perturbation appears, the jet is more and more contracted and behaves like a flat sheet with a thickness that is far less than the jet diameter. At this time, the acoustic field in the cavity is stationary. At τ=36 ms (Fig. 8.d), the sheet abruptly begins to atomise from Z~3 D_l and ejects droplets in all directions. Larger drops are ejected in the Y direction (rim atomisation). Between τ=36 ms and τ=47 ms (Fig. 8.e), the atomisation process propagates upstream up to the nozzle for these flow conditions. After

Figure 7: Visualisations of jets at a pressure node (X_{inj}=λ/4) for U_g=0 m/s, P_{ac}=3 200 Pa and a. U_l=0.3 m/s; b. U_l=0.6 m/s; c. U_l=0.8 m/s. Steady state
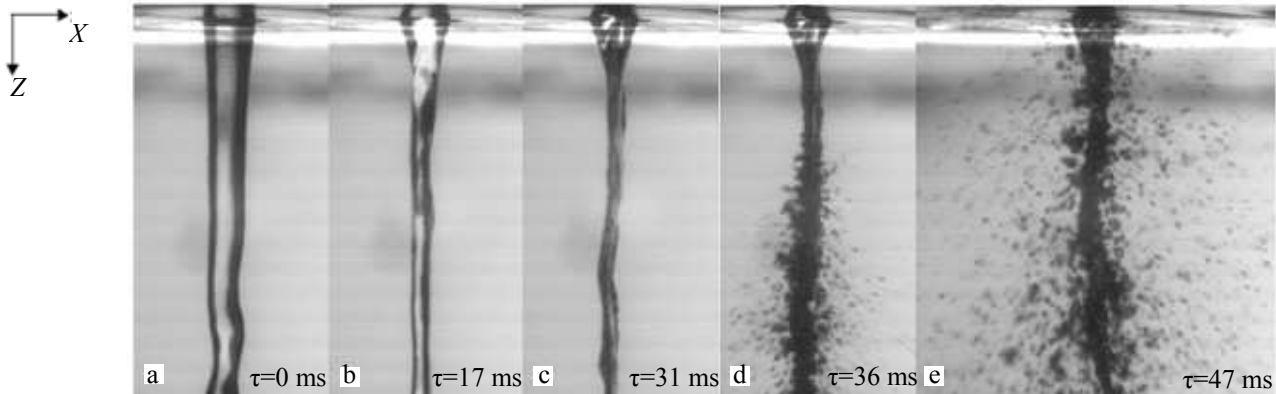

Figure 8: Time-resolved views of the liquid jet for U_g=14 m.s^{-1}, U_l=0.3 m.s^{-1}, after the start of acoustics

τ=47 ms, the sheet is in a steady state.

Similar atomisation processes are reported in the literature [8], where jets with a diameter of the order of 100 μm flatten as liquid sheets under the action of a transversal ultrasonic standing wave at 20 000 Hz. The jet diameter over the acoustic wavelength ratio is similar to the one of the present study, *i.e.* ~ 0.01. We suggest that the formation and the disintegration of the sheet are related to Faraday instabilities, for which this ratio is a similarity factor. These instabilities take place when liquid/gas or heavy gas/light gas interfaces are submitted to periodical time-modulated volume forces [9,10]. The forcing amplitude can be adjusted either to resonate the instability at harmonics of the excitation frequency or to stabilise the interface. Under these forces, the present liquid jet is squeezed on an equipotential surface of the acoustic pressure (*e.g.* in [10]) and rearranged as a liquid sheet. Further experimental investigations on the influence of P_{ac} on the sheet stability should be conducted to validate this suggestion.

6. CONCLUSIONS

The experimental investigation presented in this paper reports that the disintegration process of a cylindrical liquid jet surrounded by a co-flowing air stream can be very much affected by the presence of a standing acoustic field in the surrounding atmosphere. For injection conditions characterised by a Weber number higher than 60, the acoustic field does not significantly influence the macroscopic features of the atomisation process such as the length of the liquid core or the spray angle. This behaviour is valid whatever the position of the jet in the acoustic field. However, for Weber numbers less than 60, corresponding to the axisymmetric and non-axisymmetric Rayleigh break-up regimes according to Lasheras and Hopfinger [5] terminology, the atomisation process is very much influenced by the presence of a transverse standing acoustic field. This influence is a function of the injection conditions (gas and liquid velocities), of the acoustic field intensity as well as of the position of the jet in the acoustic field. Indeed, when the jet is located at a pressure anti-node, the presence of the acoustic field increases or reduces the jet break-up length according to the liquid and gas velocity and the acoustic field intensity. Thus, it is interesting to note that an acoustic field plays either for or against the disintegration of a air-assist liquid jet. When the jet is located at a pressure node, the disintegration process of the liquid jet is totally modified by the acoustic field that greatly increases the atomisation efficiency. Even if the acoustic field reports an influence for injection conditions that are far from those encountered in rocket engines, the present results are of paramount importance for this application where local Weber numbers may be as small as those corresponding to these injection conditions. In other words, in high Weber number conditions, the presence of an acoustic field is expected to have a non-negligible influence on liquid elements partially atomised and on drops.

NOMENCLATURE

D_l	exit diameter of the liquid tube [m]	P_{ac}	Maximum pressure fluctuations at the centre of the cavity [Pa]
D_g	external diameter of the gas nozzle [m]		
D_{gi}	internal diameter of the gas nozzle [m]	We_g	gaseous Weber number, based on the velocity differential between the air and the liquid velocity [-]
f	acoustic emission frequency [Hz]		
L_{bu}	Break-up length [m]		
L_s	distance between the nozzle exit and the beginning of the sheet [m]	X_{inj}	position of the injector in the acoustic cavity [m]
Re_l	Liquid Reynolds number based on the water orifice diameter. [-]	τ	time after start of acoustics [s]

REFERENCES

1. M. D. Klem, JANNAF Liquid Rocket Combustion Instability Panel Research Recommendations, NASA technical memorandum 103653, pp1-12, 1990
2. Candel, C. Huynh & T. Poinsot, Some Modelling Methods of Combustion Instabilities, Unsteady Combustion, F. Culick et al. Editors, Kluwer Academic Publishers, pp 83-112, 1996
3. F. Buffum & F. Williams, The Response of a Turbulent Liquid Jet to Transverse Acoustic Fields, *Proceedings of the 1967 Heat transfer and fluid mechanics institute*, eds. Stanford university press, pp 247-276, 1967
4. H. Kuttruff, Room Acoustics (third edition), E&FN SPON, 1991.
5. J. C. Lasheras & E. J. Hopfinger, Liquid Jet Instability and Atomisation in a Coaxial Gas Stream, *Annu. Rev. Fluid Mech.*, pp 275-308, 2000.
6. A. Lefebvre, Atomization and Sprays, 1989
7. S. Leroux, C. Dumouchel and M. Ledoux, The Stability Curve of Newtonian Liquid Jets, *Atomisation & Sprays vol 6, n°6*, pp 623-647, 1996.
8. K. Bauckhage, O. Andersen, S. Hansmann, W. Reich and P. Schreckenberg, Production of Fine Powders by Ultrasonic Standing Wave Atomisation, *Powder Technology*, pp 77-86, 1996.
9. D. R. Woods & S. P. Lin, Instability of a Liquid Film Flow over a Vibrating Inclined Plane, *Journal of Fluid Mechanics*, pp 391-407, 1995
10 F. Baillot, D. Durox, S. Ducruix, G. Searby and L. Boyer, Parametric Response of a Conical Flame to Acoustic Waves, *Combustion Science and Technology*, p 91-109, 1999